RSC Advances

PAPER

View Article Online
View Journal | View Issue

Cite this: *RSC Adv.*, 2020, **10**, 14972

Coordination environment evolution of Co(II) during dehydration and re-crystallization processes of $KCoPO_4 \cdot H_2O$ towards enhanced electrocatalytic oxygen evolution reaction†

Quande Che, *[a] Xiaobin Xie,[b] Qian Ma,[a] Junpeng Wang,[a] Yuanna Zhu,[a] Ruixia Shi[a] and Ping Yang *[a]

Development of efficient and stable electrodes for electrocatalytic oxygen evolution reaction (OER) is essential for energy storage and conversion applications, such as hydrogen generation from water splitting, rechargeable metal–air batteries and renewable fuel cells. Alkali metal cobalt phosphates show great potential as OER electrocatalysts. Herein, an original electrode design strategy is reported to realize an efficient OER electrocatalyst through engineering the coordination geometry of Co(II) in $KCoPO_4 \cdot H_2O$ by a facile dehydration process. Experimental result indicated that the dehydration treatment is accompanied by a structural transformation from orthorhombic $KCoPO_4 \cdot H_2O$ to hexagonal $KCoPO_4$, involving a concomitant coordination geometry evolution of Co(II) from octahedral to tetrahedral configuration. More significantly, the local structural evolution leads to an advantageous electronic effect, *i.e.* increased Co–O covalency, resulting in an enhanced intrinsic OER activity. To be specific, the as-produced $KCoPO_4$ can deliver a current density of 10 mA cm^{-2} at a low overpotential of 319 mV with a small Tafel slope of 61.8 mV dec^{-1} in alkaline electrolyte. Thus, this present research provides a new way of developing alkali metal transition-metal phosphates for efficient and stable electrocatalytic oxygen evolution reaction.

Received 25th February 2020
Accepted 6th April 2020

DOI: 10.1039/d0ra01813a

rsc.li/rsc-advances

1. Introduction

The oxygen evolution reaction (OER) is one of the crucial steps of energy storage and conversion applications, such as hydrogen generation from water splitting, rechargeable metal–air batteries and renewable fuel cells.[1–5] However, the intrinsic sluggish kinetics of the OER involving four-electron transfer requires an overpotential to drive the process.[6–8] Therefore, efficient electrocatalysts with high activity and high stability are desirable to realize its practical application.[9,10] To date, noble-metal oxides, such as RuO_2 and IrO_2 are considered to be the state-of-the-art electrocatalysts for the OER,[11,12] but their high cost, limited reserves and stability problem prevent their large-scale industrial application.[13] Currently, extensive research efforts have been focused towards the development of cost-effective transition-metal based OER catalysts.[14–20]

In particular, alkali metal cobalt phosphates have gained increasing attention due to their high activity and favorable kinetics, such as orthophosphate ($LiCoPO_4$),[21] pyrophosphate ($NaCoP_2O_7$),[22] and metaphosphate ($NaCo(PO_3)_3$).[23] The diverse orientations of phosphate ligands lead to various crystal structures, which are usually beneficial for the structural stability during OER process.[24–26] As illustrated in Fig. S2,† phosphate/pyrophosphate/metaphosphate-containing compounds have various cobalt(II) geometries including octahedral (O_h), tetrahedral (T_d) and trigonal bipyramidal (TBP), with diverse connections and low-symmetry crystal structures due to the bulky phosphate ligands. Thus, alkali metal Co phosphates with various structural configurations provide an ideal platform to design efficient and stable OER electrocatalyst. Previous research has demonstrated that the Co geometric coordination has a great impact on the OER activity of Co based phosphates. Kim *et al.* selected four Co based phosphates with various Co coordination environment, including $Na_2CoP_2O_7$ (T_d), $LiCoPO_4$ (O_h), $NaCoPO_4$ (O_h), $Li_2CoP_2O_7$ (O_h/TBP), as a platform to explore the relationship between the local coordination and the OER activity.[27] The result demonstrated that the $Na_2CoP_2O_7$ shows enhanced activity relative to $NaCoPO_4$ due to a highly distorted tetrahedral geometry. Nevertheless, Wan *et al.* subsequently reported that the $NaCo_4(PO_4)_3$ containing a rare 5

[a]School of Materials Science and Engineering, University of Jinan, Jinan 250022, P. R. China. E-mail: mse_cheqd@ujn.edu.cn; mse_yangp@ujn.edu.cn; Fax: +86 531 87974453; Tel: +86 531 89736225

[b]School of Materials Science and Engineering, Wuhan University of Technology, Wuhan 430070, P. R. China

† Electronic supplementary information (ESI) available: Experimental, XPS, XRD, SEM, TEM and computational models and methods. See DOI: 10.1039/d0ra01813a

coordinated Co(II) outperformed the $Na_2CoP_2O_7$ (T_d).[28] Besides, some other reported alkali metal cobalt phosphates, such as $LiCoPO_4$ (O_h)[21] and $NaCo(PO_3)_3$ (O_h)[23] exhibited acceptable OER activity.

Admittedly, local coordination geometry in alkali metal cobalt phosphates plays a significant role in improving their OER activity. However, there is still a lack of deep understanding of the origin of this relationship. It is well accepted that OER activity are highly dependent on both geometric configuration and electronic structure of electrocatalysts. Thus, to address this issue, there is the need for reveal the dual effect of coordination geometry of Co(II) in alkali metal cobalt phosphates. In this work, we found that the dehydration treatment of $KCoPO_4 \cdot H_2O$ is accompanied by a structural transformation from orthorhombic to hexagonal phase, involving a concomitant coordination geometry evolution of Co(II) from octahedral to tetrahedral configuration. By this, special consideration was paid to the influence of this local structural evolution on electronic structure. Experimental result and theoretical analysis indicated that the co coordination evolution increases the Co–O covalency, resulting in an enhanced OER activity. The as-resulted $KCoPO_4$ exhibited an enhanced OER activity relative to the pristine $KCoPO_4 \cdot H_2O$. Specifically, it can deliver a current density of 10 mA cm^{-2} at a low overpotential of 319 mV with a small Tafel slope of 61.8 mV dec^{-1} in alkaline electrolyte. Moreover, stability test demonstrated it can hold its catalytic OER activity for 50 h at least. Besides, to the best of our knowledge, this work for the first time demonstrated the OER performance of the hexagonal $KCoPO_4$ containing Co(II)-T_d local coordination environment. Overall, this uniqueness of this material design not only lies in an effective strategy for local coordination evolution, but more significantly it provides an ideal platform to better understand the local coordination–activity relationship for alkali metal cobalt phosphates electrocatalysts.

2. Experimental

$KCoPO_4 \cdot H_2O$ nanoplates were synthesized *via* a simple hydrothermal process. In a typical step, an aqueous solution of $CoCl_2 \cdot 6H_2O$ (0.004 mol, 30 ml) was completely added into an aqueous solution of K_2HPO_4 (0.04 mol, 30 ml) under continuous stirring. After stirred for 2 h at room temperature (25 °C), the mixture was transferred into a Teflon-lined stainless autoclave and kept at 140 °C in an electric drying box for 20 h. The resulting pink product was collected by centrifugation, rinsed with the DI water and absolute ethanol, dried at 50 °C for 12 h to obtain the $KCoPO_4 \cdot H_2O$ nanoplates.

The coordinated water molecule in $KCoPO_4 \cdot H_2O$ can be removed by heating at 300 °C under N_2 atmosphere for 3 h to obtain the dehydrated phase, *i.e.* $KCoPO_4$. The step involved in the dehydration process is illustrated in Fig. 1(a). The characterization techniques and the electrochemical measurements were explained in the ESI.†

3. Results and discussion

The XRD pattern (Fig. 2(a)) indicates the successful preparation of the $KCoPO_4 \cdot H_2O$. The diffraction peaks of the obtained powders perfectly matched to the orthorhombic-phase potassium cobalt phosphate monohydrate $KCoPO_4 \cdot H_2O$ (JCPDS no. 86-0590), while the dehydrated phase shows different crystalline structure. Upon dehydration, the $KCoPO_4 \cdot H_2O$ was transformed into hexagonal-phase $KCoPO_4$ (JCPDS no. 82-0762), as indicated in Fig. 2(b). Fig. 1(b and c) shows the crystal structures of $KCoPO_4 \cdot H_2O$ and $KCoPO_4$, respectively. It is clearly illustrated that the dehydration is accompanied by a structural transformation and re-crystalline process. Observations by the SEM (Fig. 3(a and b)) and TEM (Fig. 3(c and e)) indicate that the as-synthesized $KCoPO_4 \cdot H_2O$ and dehydrated $KCoPO_4$ exhibit plate-like nanostructures with an average size tunable from 2 to

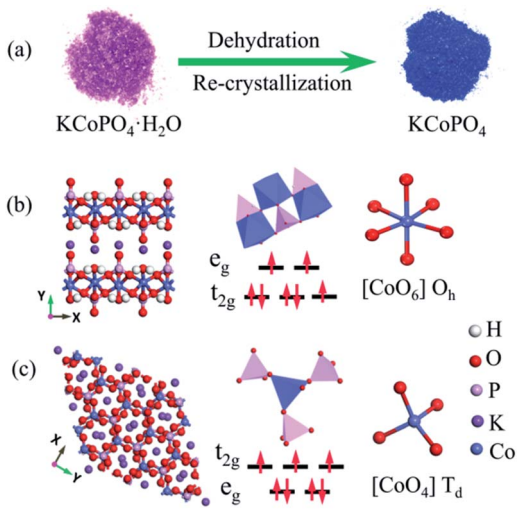

Fig. 1 (a) Schematic illustration for the dehydration and re-crystallization processes of $KCoPO_4 \cdot H_2O$. Crystal structures of (b) $KCoPO_4 \cdot H_2O$, and (c) $KCoPO_4$. The inset shows the local environment around the Co subunit (blue) and the spin state of the Co(II).

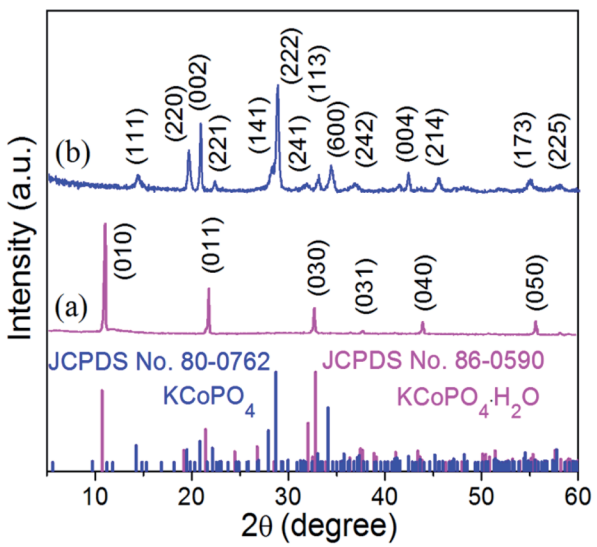

Fig. 2 XRD patterns of the as-prepared (a) $KCoPO_4 \cdot H_2O$ (JCPDS no. 86-0590), and (b) $KCoPO_4$ (JCPDS no. 82-0762), respectively.

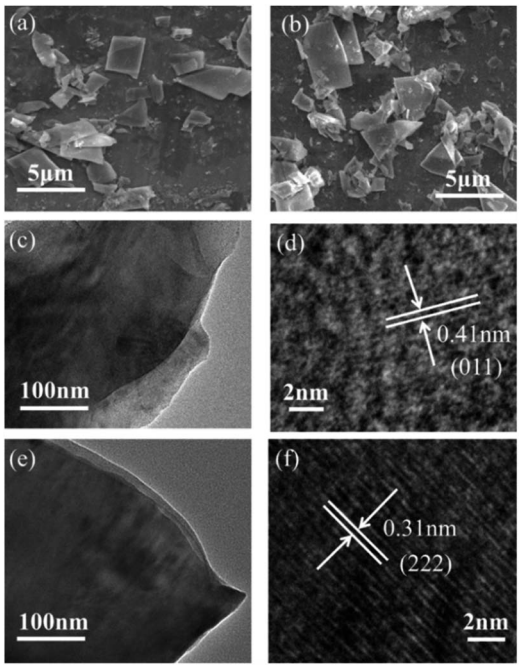

Fig. 3 SEM images of the as-prepared (a) $KCoPO_4 \cdot H_2O$, and (b) $KCoPO_4$. TEM (c and e) and HRTEM (d and f) images of $KCoPO_4 \cdot H_2O$ and $KCoPO_4$, respectively.

5 μm. Furthermore, the HRTEM images show the interlayer *d* spacing of 0.41 nm (Fig. 3(d)) and 0.31 nm (Fig. 3(f)) nm of the two phases, which are consistent with the XRD data.

Thermogravimetric analysis (TGA) was carried out under flowing N_2 to further demonstrate the dehydration and recrystalline process of $KCoPO_4 \cdot H_2O$, as shown in Fig. 4(a). The TG curve shows a sharp weight loss of 8.61%, and is characterized by a strong endothermic DTG peak at 195.7 °C, which corresponds to the loss of coordinated water molecule in $KCoPO_4 \cdot H_2O$ (calcd: 8.53%). There is no weight after that, indicating it transforms to be a stable $KCoPO_4$.

Significantly, upon dehydration, the coordination environment around Co(II) changed from octahedral to tetrahedral configuration, which is demonstrated by a concomitant color change from pink to blue. In other words, The Co–O bond from the oxygen in the water molecule coordinated with Co(II) is lost during dehydration, leading to the coordination of the Co(II) becomes to tetrahedral. The diffuse-reflectance solid-state UV-vis spectra of the two phases was shown in Fig. 4(b). The spectrum of $KCoPO_4 \cdot H_2O$ shows a broad band located at approximately 539 nm, which correspond to the $^4T_{1g}$ (F) $^4A_{2g}$ (P) transition (ν_3 band) of high-spin Co(II) in octahedral $[CoO_5(H_2O)]^{2+}$,[29] while for $KCoPO_4$ the bands located at about 526 nm, 575 nm, and 615 nm are assigned to the $^4A_{2g}$ (F) $^4T_1$ (P) of high-spin tetrahedral Co(II).[30] Thus, the UV-vis spectra suggests a structural conversion from octahedral to tetrahedral coordination. Fig. 1(b and c) shows the local coordination environment and the spin state of Co(II) in the two phases, respectively. As mentioned above, the Co geometric coordination has a great impact on the OER activity of Co based phosphates. Therefore, the coordination environment evolution of Co(II) in the two phases motivate us to explore the corresponding change of their OER performance and the original relationship between coordination configuration with OER activity of Co phosphates. However, just knowing the structural transformation is far from enough, there is the need for further efforts to reveal the corresponding electronic effect.

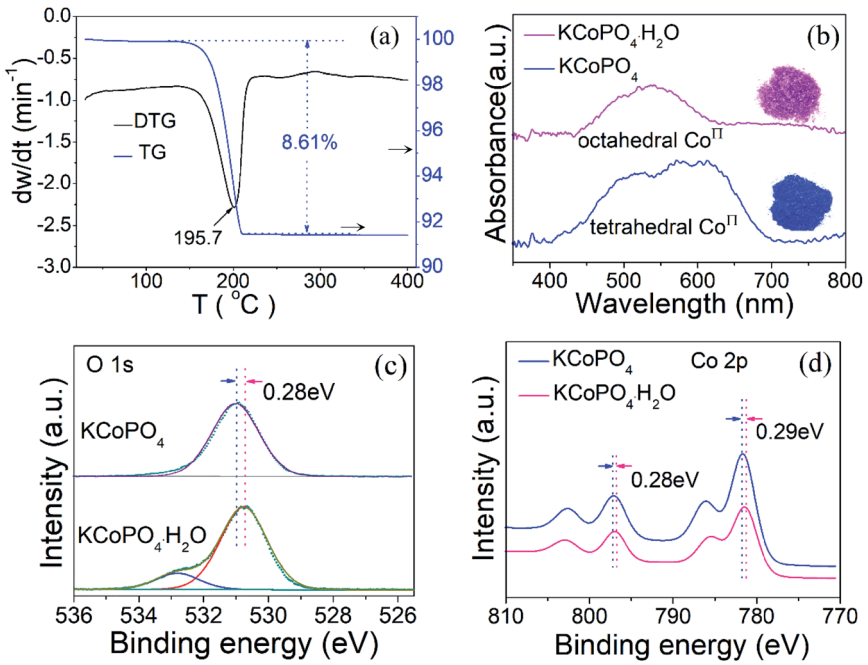

Fig. 4 (a) TGA/DTG curves of the $KCoPO_4 \cdot H_2O$ nanoplates. (b) UV-vis spectra of $KCoPO_4 \cdot H_2O$ and $KCoPO_4$. High-resolution XPS spectra for (c) O 1s, and (d) Co 2p of the $KCoPO_4 \cdot H_2O$ and $KCoPO_4$, respectively.

The chemical compositions and bonding states in the as-prepared $KCoPO_4 \cdot H_2O$ and dehydrated $KCoPO_4$ were examined by XPS, which contributes to estimate the electron states of Co in the two phases, and in turn is conductive to reveal the electronic effect of coordination environment evolution of Co(II) on OER activity. First, the full survey spectra (Fig. S3(a and b)†) indicates the presence of cobalt (Co 2p), phosphorus (P 2p), oxygen (O 1s), potassium (K 2p) from both of the two compounds. Furthermore, the O 1s spectrum of $KCoPO_4 \cdot H_2O$ (Fig. 4(c)) fitted into two peaks situated at 530.7 eV and 532.8 eV can be ascribed to the P–O bonds and coordinated water molecule, respectively,[31] while for $KCoPO_4$ only lattice oxygen can be tested, as illustrated by the peak located at about 531.0 eV. More significantly, it is found that there is a positive shift (about 0.3 eV) of binding energy for oxygen after the dehydration process, which indicates the increased valence state of oxygen in $KCoPO_4$. Similarly, the valence state of cobalt increases on dehydration, as confirmed by the positive shift (about 0.3 eV) of binding energy, as shown in (Fig. 4(d)). Specifically, the Co 2p spectrum of $KCoPO_4 \cdot H_2O$ fitted into two peaks located at 796.8and 781.3 eV, while for $KCoPO_4$ the peaks situated at 797.1 and 781.6 eV, respectively. Besides, the Co 2p spectra of the two compounds indicate the Co^{2+} oxidation state of cobalt in both of them.[32] In a word, the XPS result suggests the increased degree of Co–O hybridization, *i.e.* Co–O covalency in $KCoPO_4$.

Based on the above characterizations including crystal structure and chemical bonding states, it is clearly indicated that the dehydration process of $KCoPO_4 \cdot H_2O$ is accompanied by a structural transformation from orthorhombic-phase to hexagonal-phase. More significantly, the local coordination geometry evolution of Co(II) from octahedral to tetrahedral configuration increases the Co–O covalency. Previous research demonstrated that the geometric configuration and electronic structure of cobalt phosphates can largely influence its OER catalytic activity.[33,34] Therefore, the local Co geometry evolution with increased Co–O covalency may imply an enhanced OER activity.

The OER performance of the as-prepared two compounds was evaluated *via* linear scanning voltammetry (LSV) using a conventional three-electrode system at a scan rate of 5 mV s^{-1} in 1.0 M KOH (electrochemical measurements, see details in ESI†). Fig. 5(a) shows the LSV curves of the as-prepared $KCoPO_4$, together with the $KCoPO_4 \cdot H_2O$, and RuO_2 for comparison. As illustrated in Fig. 5(a), the $KCoPO_4 \cdot H_2O$ requires 387 mV overpotential to reach a current density of 10 mA cm^{-2}. On $KCoPO_4$, the overpotential greatly decreased to 319 mV, which is even comparable to that of the reference sample (309 mV for noble RuO_2). Not only that, the catalytic performance of $KCoPO_4$ is comparable to or even superior to many recently reported transition-metal phosphate based electrocatalysts (the detailed comparison can be seen in Table S3, ESI†). Besides, a smaller Tafel slope of 61.8 mV dec^{-1} of $KCoPO_4$ than that of $KCoPO_4 \cdot H_2O$ (66.2 mV dec^{-1}) indicates the favorable reaction kinetic for OER, as shown in Fig. 5(b). It could also be inferred from the electrochemical impedance spectroscopy (EIS) result (Fig. 5(c)). An equivalent circuit model was suggested, as shown in inset of Fig. 5(c). The charge transfer resistance (R_{ct}), was tested to be 36.1 Ω for $KCoPO_4$, much lower than 139.9 Ω for $KCoPO_4 \cdot H_2O$. Furthermore, CV curves with different scan rates were recorded to evaluate electrochemically active surface area (ECSA) of the two compounds, as shown in Fig. 6(a and b). It can be evaluated

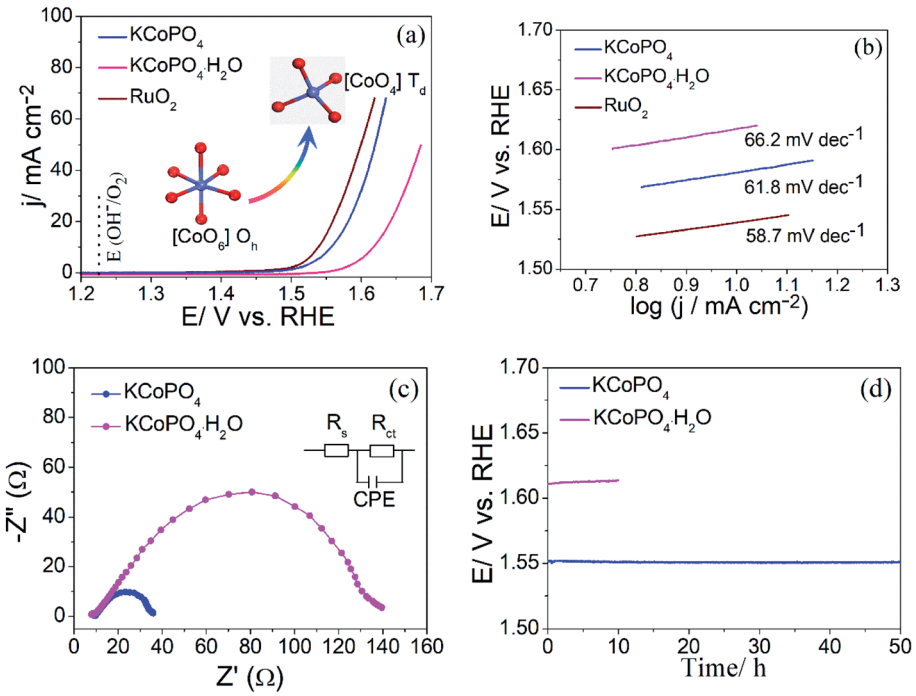

Fig. 5 OER performance of the as-prepared $KCoPO_4 \cdot H_2O$, $KCoPO_4$, and RuO_2. (a) LSV curves, (b) corresponding Tafel plots, (c) EIS spectra, and (d) chronopotentiometric curves at 10 mA cm^{-2}.

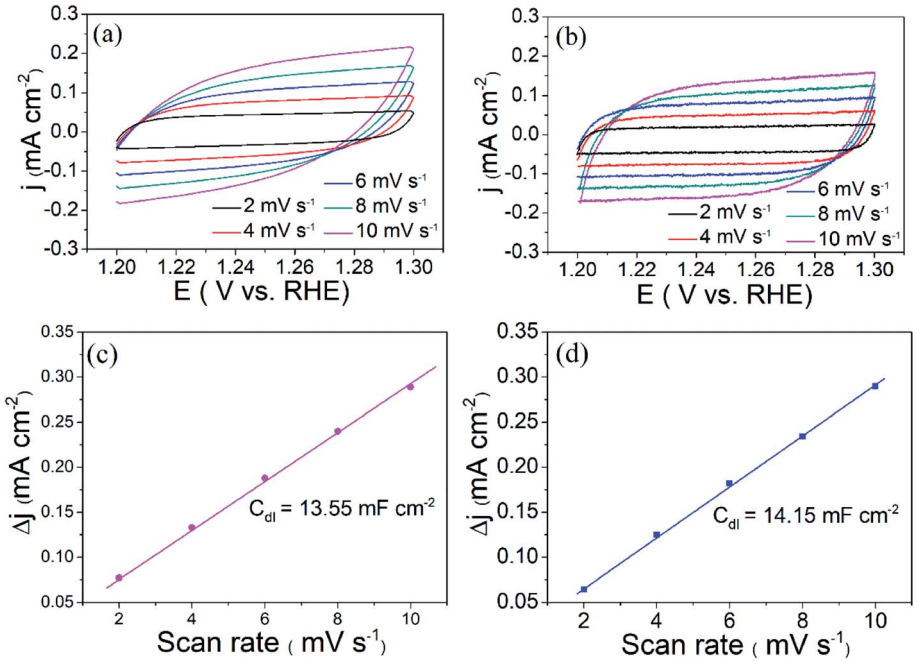

Fig. 6 Cyclic voltammetry curves of (a) $KCoPO_4 \cdot H_2O$, and (b) $KCoPO_4$ in 1 M KOH with different scan rates. Δj of as-above electrodes plotted against scan rates, (c) $KCoPO_4 \cdot H_2O$, and (d) $KCoPO_4$.

with the electrochemical double-layer capacitance (C_{dl}), which is determined by current density differences plotted against various scan rates. Specifically, the C_{dl} of $KCoPO_4$ was calculated to be 14.15 mF cm^{-2}, which is very close to that of $KCoPO_4 \cdot H_2O$ (13.55 mF cm^{-2}), indicating an equivalent ECSA value of them. Therefore, it is proposed that the transformation of $KCoPO_4 \cdot H_2O$ to $KCoPO_4$ lead to the enhanced intrinsic OER activity. In order to estimate the intrinsic activity, turnover frequency (TOF) was calculated for them. The TOF value of $KCoPO_4$, $KCoPO_4 \cdot H_2O$ and RuO_2 were 0.0635 s^{-1}, 0.0413 s^{-1}, 0.015 s^{-1}, respectively, which are comparable with the previously reported values.[35] Such a high TOF value means a very high intrinsic activity of $KCoPO_4$.

Based on the above comparison study on structural transformation and OER performance evaluation, it is suggested that the enhanced OER activity is mainly derived from the electronic effect of local Co(II) geometry, *i.e.* the increased Co–O covalency.

In addition, the stability measurement for the as-prepared $KCoPO_4$ manifests that the long-term durability requirement can be met. The chronopotentiometry result of $KCoPO_4$ at a constant 10 mA cm^{-2}, as shown in Fig. 5(d), indicating the potential kept stable at ~1.55 V in an OER process up to 50 h. The LSV curve after 50 h test exhibited a negligible shift, as shown in Fig. S4.† Besides, the structural characterizations, as illustrated in Fig. S5,† further demonstrated the stability.

Based on the above analysis, it is suggested that the distinct OER activity is associated with the local electronic structure modulation by coordination environment evolution of Co(II). In other words, the local Co geometry evolution from octahedral to tetrahedral configuration with increased Co–O covalency result in an enhanced OER activity. This analysis is consistent with the previous research. Recent studies demonstrated that the increased Co–O covalency promotes the interfacial charge transfer between Co and oxygen intermediates, resulting in an enhanced OER kinetics.[36–39] To further confirm the electronic effect, first-principles density functional theory plus Hubbard U (DFT+U) calculations were performed on the two compounds (computational models and methods can be seen in the ESI†). The calculated partial densities of the states (pDOS) of Co 3d and O 2p band are shown in Fig. 7(a and b). As a feasible descriptor for OER activity, the electronic parameter, *i.e.*, O 2p

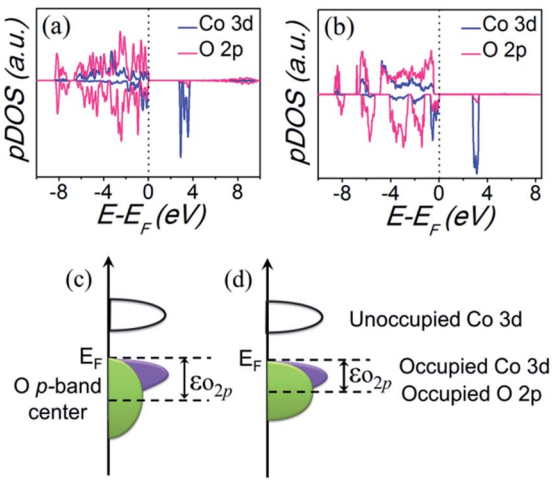

Fig. 7 Computed partial electronic density of states (pDOS) of Co 3d and O 2p band of (a) $KCoPO_4 \cdot H_2O$, and (b) $KCoPO_4$. Illustration of the relationships between Co 3d and O 2p band of (c) $KCoPO_4 \cdot H_2O$, and (d) $KCoPO_4$, respectively.

band center (ε_{O2p}) can be extracted out from the calculated pDOS,[40–42] which also indicates the degree of Co–O hybridization, as illustrated in Fig. 7(c and d). In specific, a larger ε_{O2p} signify greater covalency and better OER activity. It is observed that the calculated ε_{O2p} of $KCoPO_4$ (−2.95 eV) is more positive than that of $KCoPO_4 \cdot H_2O$ (−3.24 eV), indicating the increased Co–O covalency, which is confirmed by the XPS analysis.

4. Conclusions

In summary, $KCoPO_4 \cdot H_2O$ nanoplates were successfully synthesized *via* a hydrothermal process. The coordination water molecule in $KCoPO_4 \cdot H_2O$ can be removed by heating at 300 °C under N_2 atmosphere to obtain the dehydrated $KCoPO_4$. Significantly, the dehydration process is accompanied by a phase transformation, and a local coordination environment evolution of Co(II) from octahedral to tetrahedral configuration, which increases the Co–O covalency, resulting in an enhanced OER activity. In specific, the dehydrated $KCoPO_4$ can deliver a current density of 10 mA cm^{-2} at a low overpotential of 319 mV with a small Tafel slope of 61.8 mV dec^{-1} in alkaline electrolyte. Thus, this present research enlightens a new way of developing alkali metal transition-metal phosphates for efficient and stable water oxidation.

Conflicts of interest

There are no conflicts to declare.

Acknowledgements

The work was supported by the National Natural Science Foundation of China (51602128), the Research Foundation from University of Jinan (XKY1401, XBS1508, XBH1504).

Notes and references

1 T. Fujimura, W. Hikima, Y. Fukunaka and T. Homma, *Electrochem. Commun.*, 2019, **101**, 43.
2 W. Yang, K.-Y. Kim, P. E. Saikaly and B. E. Logan, *Energy Environ. Sci.*, 2017, **10**, 1025.
3 C. Liu, J. Tang, H. M. Chen, B. Liu and P. Yang, *Nano Lett.*, 2013, **13**, 2989.
4 Y. Liu, X. Liang, L. Gu, Y. Zhang, G.-D. Li, X. Zou and J.-S. Chen, *Nat. Commun.*, 2018, **9**, 2609.
5 A. Pirkarami, S. Rasouli and E. Ghasemi, *Appl. Catal., B*, 2019, **241**, 28.
6 S. Fukuzumi, Y. M. Lee and W. Nam, *Dalton Trans.*, 2019, **48**, 779.
7 Y. Q. Li, C. Wang, M. Cui, S. R. Chen and T. L. Ma, *Catal. Commun.*, 2019, **131**, 105800.
8 Y. Lee, J. Suntivich, K. J. May, E. E. Perry and Y. Shao-Horn, *J. Phys. Chem. Lett.*, 2012, **3**, 399.
9 J. Kibsgaard and I. Chorkendorff, *Nat. Energy*, 2019, **4**, 430.
10 Y. Zhang, X. Wang, F. Luo, Y. Tan, L. Zeng, B. Fang and A. Liu, *Appl. Catal., B*, 2019, **256**, 117852.
11 L. C. Seitz, C. F. Dickens, K. Nishio, Y. Hikita, J. Montoya, A. Doyle, C. Kirk, A. Vojvodic, H. Y. Hwang, J. K. Norskov and T. F. Jaramillo, *Science*, 2016, **353**, 1011.
12 J. Yi, W. H. Lee, C. H. Choi, Y. Lee, K. S. Park, B. K. Min, Y. J. Hwang and H. S. Oh, *Electrochem. Commun.*, 2019, **104**, 106469.
13 J. Jiang, Q. Liu, C. Zeng and L. Ai, *J. Mater. Chem. A*, 2017, **5**, 16929.
14 X. F. Zhang, A. X. Shan, S. B. Duan, H. F. Zhao, R. M. Wang and W.-M. Lau, *RSC Adv.*, 2019, **9**, 40811.
15 I. V. Odynets, N. Y. Strutynska, J. Z. Li, W. Han, I. V. Zatovsky and N. I. Klyui, *Dalton Trans.*, 2018, **47**, 15703.
16 S. S. Zhu, J. L. Lei, Y. H. Qin, L. N. Zhang and L. J. Lu, *RSC Adv.*, 2019, **9**, 13269.
17 F. Dionigi and P. Strasser, *Adv. Energy Mater.*, 2016, **6**, 1600621.
18 Y. W. Liu, C. Xiao, M. J. Lyu, Y. Lin, W. Z. Cai, P. C. Huang, W. Tong, Y. M. Zou and Y. Xie, *Angew. Chem., Int. Ed.*, 2015, **54**, 1123.
19 M. Huynh, C. Y. Shi, S. J. L. Billinge and D. G. Nocera, *J. Am. Chem. Soc.*, 2015, **137**, 14887.
20 J. Y. Wang, X. Teng, Y. L. Niu, L. X. Guo, J. F. Kong, X. M. He and Z. F. Chen, *RSC Adv.*, 2019, **9**, 21679.
21 S. W. Lee, C. Carlton, M. Risch, Y. Surendranath, S. Chen, S. Furutsuki, A. Yamada, D. G. Nocera and Y. Shao-Horn, *J. Am. Chem. Soc.*, 2012, **134**, 16959.
22 L. Q. Gui, X. Y. Miao, C. J. Lei, K. L. Wang, W. Zhou, B. B. He, Q. Wang and L. Zhao, *Chem.–Eur. J.*, 2019, **25**, 11007.
23 R. Gond, D. K. Singh, M. Eswaramoorthy and P. Barpanda, *Angew. Chem., Int. Ed.*, 2019, **131**, 8418.
24 T. H. Zhou, Y. H. Du, D. P. Wang, S. M. Yin, W. G. Tu, Z. Chen, A. Borgna and R. Xu, *ACS Catal.*, 2017, **7**, 6000.
25 X. L. Hu, S. Piccinin, A. Laio and S. Fabris, *ACS Nano*, 2012, **6**, 10497.
26 M. W. Kanan, Y. Surendranath and D. G. Nocera, *Chem. Soc. Rev.*, 2009, **38**, 109.
27 H. Kim, J. Park, I. Park, K. Jin, S. E. Jerng, S. H. Kim, K. T. Nam and K. Kang, *Nat. Commun.*, 2015, **6**, 8253.
28 H. Wan, R. Z. Ma, X. H. Liu, J. L. Pan, H. D. Wang, S. Q. Liang, G. Z. Qiu and T. Sasaki, *ACS Energy Lett.*, 2018, **3**, 1254.
29 B. M. Weckhuysen, D. Baetens and R. A. Schoonheydt, *Angew. Chem., Int. Ed.*, 2000, **39**, 3419.
30 D. Grandjean, A. M. Beale, A. V. Petukhov and B. M. Weckhuysen, *J. Am. Chem. Soc.*, 2005, **127**, 14454.
31 C. Z. Wei, C. Cheng, S. S. Wang, Y. Z. Xu, J. D. Wang and H. Pang, *Chem.–Asian J.*, 2015, **10**, 1731.
32 B. J. Tan, K. J. Klabunde and P. M. Sherwood, *J. Am. Chem. Soc.*, 1991, **113**, 855.
33 I. Roger, M. A. Shipman and M. D. Symes, *Nat. Rev. Chem.*, 2017, **1**, 0003.
34 Y. Surendranath, M. W. Kanan and D. G. Nocera, *J. Am. Chem. Soc.*, 2010, **132**, 16501.
35 H. F. Du, W. Ai, Z. L. Zhao, Y. Chen, X. Xu, C. J. Zou, L. S. Wu, L. Su, K. K. Nan, T. Yu and C. M. Li, *Small*, 2018, **14**, 1801068.

36 S. Yagi, I. Yamada, H. Tsukasaki, A. Seno, M. Murakami, H. Fujii, H. Chen, N. Umezawa, H. Abe, N. Nishiyama and S. Mori, *Nat. Commun.*, 2015, **6**, 8249.

37 J. T. Mefford, X. Rong, A. M. Abakumov, W. G. Hardin, S. Dai, A. M. Kolpak, K. P. Johnston and K. J. Stevenson, *Nat. Commun.*, 2016, **7**, 11053.

38 J. Suntivich, K. J. May, H. A. Gasteiger, J. B. Goodenough and Y. Shao-Horn, *Science*, 2011, **334**, 1383.

39 Y. Duan, S. N. Sun, S. B. Xi, X. Ren, Y. Zhou, G. L. Zhang, H. T. Yang, Y. H. Du and Z. C. Xu, *Chem. Mater.*, 2019, **29**, 10534.

40 J. G. Lee, J. Hwang, H. J. Hwang, O. S. Jeon, J. Jang, O. Kwon, Y. Lee, B. Han and Y. G. Shul, *J. Am. Chem. Soc.*, 2016, **138**, 3541.

41 W. T. Hong, K. A. Stoerzinger, Y. L. Lee, L. Giordano, A. Grimaud, A. M. Johnson, J. Hwang, E. J. Crumlin, W. L. Yang and Y. Shao-Horn, *Energy Environ. Sci.*, 2017, **10**, 2190.

42 Y. Zhou, S. N. Sun, J. J. Song, S. B. Xi, B. Chen, Y. H. Du, A. C. Fisher, F. Y. Cheng, X. Wang, H. Zhang and Z. C. Xu, *Adv. Mater.*, 2018, **30**, 1802912.

